Charge transfer in heterostructures of T and H transition metal dichalcogenides

Irián Sánchez-Ramírez,[1,2] Maia G. Vergniory,[1,3] and Fernando de Juan[1,2,4]

[1]*Donostia International Physics Center, P. Manuel de Lardizabal 4, 20018 Donostia-San Sebastian, Spain*

[2]*Departamento de Fisica de Materiales, Facultad de Ciencias Quimicas, Universidad del Pais Vasco (UPV-EHU), P. Manuel de Lardizabal 3, 20018 Donostia-San Sebastian, Spain*

[3]*Max Planck Institute for Chemical Physics of Solids, 01187 Dresden, Germany*

[4]*IKERBASQUE, Basque Foundation for Science, Maria Diaz de Haro 3, 48013 Bilbao, Spain*

(Received 3 July 2024; revised 15 October 2024; accepted 21 October 2024; published 19 November 2024)

The $\sqrt{13}\times\sqrt{13}$ charge density wave state of the T polytype of MX_2 (M = Nb, Ta, X = S, Se) is known to host a half-filled flat band which electronic correlations drive into a Mott insulating state. When T polytypes are coupled to strongly metallic H polytypes, such as in T/H bilayer heterostructures or the bulk $4H_b$ polytype, charge transfer can destabilize the Mott state, but quantifying its magnitude has been a source of controversy. In this work, we perform a systematic *ab initio* study of charge transfer for all experimentally relevant T/H bilayers and bulk $4H_b$ structures. In all cases we find charge transfer from T to H layers which depends strongly on the interlayer distance but weakly on the Hubbard interaction. Additionally, Se compounds display smaller charge transfer than S compounds, and $4H_b$ bulk polytypes display more charge transfer than isolated bilayers. We rationalize these findings in terms of band structure properties and argue they might explain differences between compounds observed experimentally. Our work reveals the tendency to Mott insulation and the origin of superconductivity may vary significantly across the family of T/H heterostructures.

DOI: 10.1103/PhysRevB.110.195138

I. INTRODUCTION

Metallic transition metal dichalcogenides (TMDs) MX_2 (M=Nb, Ta, X=S, Se) [1–3] are layered compounds made by stacking two basic MX_2 monolayer units known as H, with trigonal prismatic coordination of the metal, and T, with octahedral coordination [4]. Despite both having partially filled metal d-orbital bands, the low-temperature properties of these building blocks are markedly different: While H layers show weak charge density waves (CDW) and remain metallic and often superconducting [2], T layers are understood to be Mott insulators [5]. The reason for this is the strong Star of David (SOD) $\sqrt{13}\times\sqrt{13}$ CDW reconstruction [6], which gaps out most of the Fermi surface, leaving a half-filled flat band at the Fermi level which derives from an isolated orbital located at the SOD centers. The presence of even moderate Coulomb repulsion in these orbitals should thus drive this system to a Mott insulator state [5] and perhaps a spin liquid [7]. The realization of such states in the bulk $1T$ polytype, made of stacked T layers, is, however, complicated by interlayer tunneling and the many possible CDW stacking patterns [8]. However, the recent synthesis of T monolayers [9] has provided stronger support for the Mott insulator scenario.

TMD heterostructures alternating T and H layers provide an interesting alternative to put the hypothesis of the Mott insulator to test. In these structures the SOD moments from the T layer are coupled to the metallic electrons from the H layer, providing a natural realization of a CDW-induced Kondo lattice. Recently synthesized T/H bilayers have, indeed, shown prominent zero-bias peaks in $TaSe_2$ [9,10], TaS_2 [11,12], and $NbSe_2$ [13,14] which have been interpreted as the Kondo effect. In addition to such isolated bilayers, two naturally occurring bulk polytypes formed by alternating T and H layers also exist, known as $4H_b$ [15,16] (with an inversion-symmetric stacking of T/H bilayers) and $6R$ [17,18] (with an inversion-breaking rhombohedral stacking). Interest in such compounds has recently been revived because, in addition to displaying similar Kondo effects [19,20], $4H_b$-TaS_2 shows unexpected signatures of unconventional superconductivity [21]: spontaneous breaking of time-reversal symmetry at T_c [22], spontaneous vortices in the superconducting state [23], superconducting edge modes [24], and transport evidence of a two-component order parameter [25,26].

The interpretation of all of these experiments and the relevance of the Mott insulator picture is critically dependent on two properties of the T/H interface which have remained under certain controversy: the interlayer hybridization V and the charge transfer $\Delta C = (C_H - C_T)/2$, where $C_H = C_T$ in vacuum and the factor $1/2$ accounts for double counting. Indeed, the T layer can remain a Mott insulator only if the flat band is nearly half filled, but since the work function of the H layer is larger than that of the T layer, some amount of charge transfer from T to H is expected [27–29]. The Kondo effect similarly can survive only a certain charge transfer, and in addition it is realized for only a critical hybridization $V > V_c$. Superconductivity is also expected to be very different depending on whether the T layer contributes magnetic moments or not. A recent work advocated the picture of a doped Mott insulator with negligible V [30]. Importantly, the effect of interlayer charge transfer in bulk $4H_b$ compounds has not been addressed to date, nor has the potential variability in the different members of the family, TaS_2, $TaSe_2$, and $NbSe_2$.

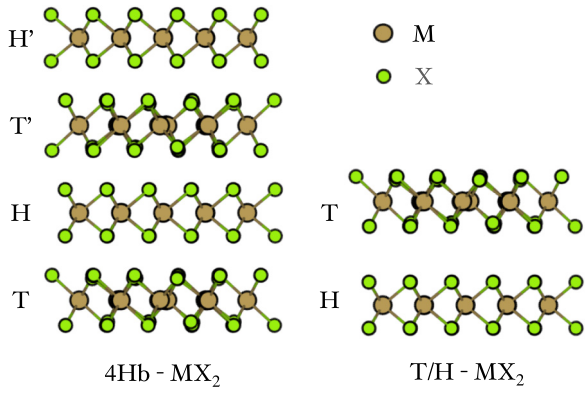

FIG. 1. Bulk $4H_b$ (left) and bilayer T/H (right) MX_2 (M=Nb, Ta, X=S, Se) structures considered in this work.

In this work, we conduct a systematic study of charge transfer across all these compounds, exploring its correlation with work function mismatch, van der Waals corrections, Hubbard's U parameter, and interlayer spacing. Our calculations reveal that the influence of U and van der Waals effects is minimal, while we observe that charge transfer is inversely related to the distance between layers and directly linked to the mismatch in work functions. In addition, we find the general trend that Se compounds display smaller charge transfer than S compounds, and $4H_b$ bulk polytypes display more charge transfer than isolated bilayers.

II. CHARGE TRANSFER IN T/H STRUCTURES

Early works [27–29] already anticipated that charge transfer from the T to the H layers must be present in bulk $4H_b$ TMDs. T/H bilayer and bulk $4H_b$-MX_2 structures are shown in Fig. 1. At high temperatures where the CDW in the T layers is incommensurate, the change in the CDW wave vector compared to bulk $1T$ polytypes was used to estimate a transfer of $0.12e^-$ per formula unit [27] ($1.56e^-$ per SOD) in $4H_b$-TaS_2, and a similar estimate leads to $1.20e^-$ per SOD for $TaSe_2$. Similar theoretical estimates [29] for $4H_b$-TaS_2 similarly ranged between 1.04 and $1.43e^-$ per SOD. Charge transfer of this magnitude was also reported to be consistent with changes in the optical conductivity in both $4H_b$ and $6R$ polytypes [28]. More recent angle-resolved photoelectron spectroscopy experiments estimated $0.92e^-$ per SOD in $4H_b$-TaS_2 [31]. All these early estimates are thus consistent with a nearly empty flat band.

Recent *ab initio* calculations in the high-temperature state without CDW [32,33] also suggest charge transfer from T to H, but given the strong band reconstruction due to the CDW, it is important to perform these calculations in the CDW state. Such calculations [20,24] for a T/H bilayer of TaS_2 still report a fully empty flat band, while a bilayer T on monolayer H was reported to have $0.31e^-$ per SOD cell [34]. For $TaSe_2$, a value of $0.32e^-$ per SOD cell was reported [10], while for $NbSe_2$ a value of $0.17e^-$ was calculated [35]. A recent study emphasized the importance of the stacking distance for charge transfer [30], revealing that ΔC ranges from 0.4 to 1 in TaS_2 as the interlayer distance goes from 7 to 5.8 Å.

Given such variability and the fact that isolated bilayers on substrates may not stack with the same interlayer distance as bulk $4H_b$ compounds, it is important to study the distance dependence in detail for $TaSe_2$ and $NbSe_2$. Differences may be expected because the flat band in the Se compounds is significantly closer to the CDW valence bands compared to the S compounds. For $NbSe_2$ one experiment has claimed [14] a charge transfer with a sign opposite to that of the Ta compounds. It is also important to take into account the details of the different *ab initio* calculations done for the Ta compounds [36–42], for example, because the exact position of the flat band within the CDW gap is known to depend on the functional used [43], which can influence charge transfer. Including the Hubbard interaction and explicitly accounting for magnetic states with spin-split bands [43–47] can similarly affect the charge transfer.

Finally, note that in the context of correlated systems the term "charge transfer" is often used to emphasize the distinction between Mott and charge transfer insulators [48]. In that case, the term refers to charge transfer between correlated d-derived bands and the dispersive p-derived bands of the same compound. In TMDs this phenomenon may also be relevant, at least for some compounds like $1T$-$NbSe_2$ or $1T$-$TaSe_xTe_{1-x}$, in which the flat band may overlap with the p-derived states [13,43,49]. In our work, unless specified otherwise, charge transfer will instead refer to interlayer charge transfer between the T and the H layers.

A. *Ab initio* methods

The aim of this work is to provide a systematic study of the interlayer charge transfer between T and H MX_2 layers. The workflow used to carry out said study is as follows: (1) single-layer in-plane structure relaxation for H and T layers, (2) single-layer work function calculation for H and T layers, (3) T/H bilayer relaxation, first relaxing in the $\hat{z}$ direction, followed by a subsequent in-plane relaxation, (4) charge transfer calculation for bilayers (in this step we explore different parameters, such as Hubbard's U, van der Waals corrections, and interlayer distance dependence), and (5) $4H_b$ charge transfer calculation using step 2 structures and experimental distances. The purpose of this workflow is to identify trends between different factors affecting *ab initio* calculations and experimental measurements, with the aim of understanding the overall behavior of charge transfer under different conditions.

All calculations were performed using the Vienna Ab initio Simulation Package (VASP) [50,51], version 6.2.1, with projector augmented wave pseudopotentials within the Perdew-Burke-Ernzerhof parametrization [52]. For steps 1 and 3, the relaxation was conducted by using the conjugate-gradient algorithm as implemented in VASP, keeping the cell shape and volume fixed while letting atomic positions relax. For steps 1–4, calculations were found to be well converged with a 480 eV kinetic cutoff and a Γ-centered $15\times15\times1$ k mesh. Meanwhile, for step 5, the self-consistent calculations were found to be well converged with a 480 eV kinetic cutoff and a Γ-centered $13\times13\times3$ k mesh. In step 4, when van der Waals corrections were considered, the DFT-D3 method [53] with zero damping was used. Also in step 4, in order

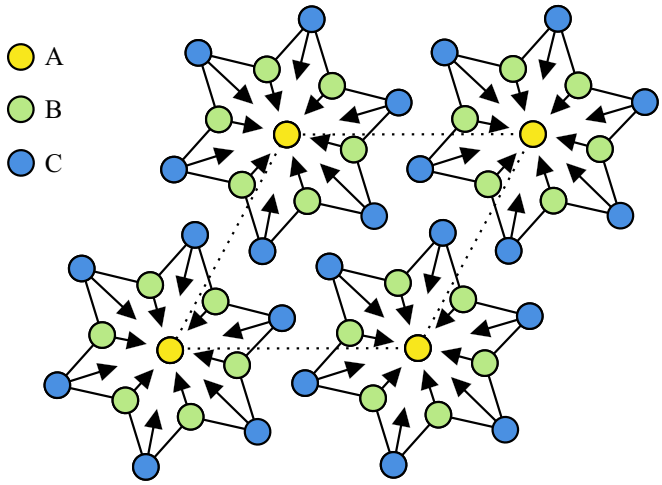

FIG. 2. Lattice structure of the SOD CDW distortion of the T layers. A, B, and C inequivalent metal sites are marked in yellow, green, and blue, respectively. Black arrows show their displacements, while the dotted line marks the CDW unit cell.

to study the effect of Coulomb repulsion, the DFT+U rotationally invariant approach [54] was followed by setting different effective on-site U Coulomb interactions in M's d orbitals with $J = 0$. These DFT+U calculations are the only collinear spin-polarized ones. The initial magnetization was set to $1.4\mu_B$ for the central Ta/Nb atom (atom A; see Sec. II B) and zero for the remaining atoms. This choice is based on prior studies suggesting that the predominant magnetic moment is concentrated at the center of the SOD [38] and that the total magnetic moment is typically around $1\mu_B$ [44,46]. The initial value of magnetization is taken to be slightly larger than the expected result because this is expected to improve convergence [55]. Atom-projected band structures were obtained using the PYPROCAR [56] package for PYTHON.

B. Charge density wave distortions

The $\sqrt{13}\times\sqrt{13}$ SOD CDW structure is shown in Fig. 2. There are three types of symmetry-equivalent M sites, labeled A, B, and C hereafter, with multiplicities 1, 6, and 6 respectively. The structure is parameterized by three independent displacements $\vec{u}_i$ with $i = A, B, C$, as shown in Fig. 2 ($|\vec{u}_A| = 0$ by symmetry). In Table I we present the displacements for each equivalent metal site in each T-MX_2 from the bilayers considered. In Appendix A we present a graphic depiction of these displacements from the T layer of the bilayer for the four compounds (Fig. 10) along with a brief note on how we obtained the CDW positions.

C. Work function analysis

We define the work function as the absolute Fermi level with respect to vacuum. Different work functions between two structures indicate misaligned Fermi levels and can be used for a qualitative estimate of charge transfer.

To compute the work functions, we perform a self-consistent calculation of the monolayer in a unit cell with ≈20 AA of vacuum in the normal direction. From this calculation we extract the local potential $V(\vec{r})$ and define the work function as

$$W = V_{\text{vac}} - E_F, \tag{1}$$

where V_{vac} is the value of $V(\vec{r})$ in vacuum. We present the work functions for both the T and H polytypes of all TMDs considered in Table I. The H work function is greater than the T work function for all TMDs, which suggests that the charge transfer will occur from T to H layer. In Table I we can already see some trends: M=Ta compounds have an overall smaller work function than M=Nb, which is also the case for X=Se when compared with X=S ones. In Sec. II D we will see how this affects the charge transfer.

TABLE I. Displacements for each inequivalent metallic position $\vec{u}_i$, with $i = A, B, C$, interlayer distance d, work functions (WFs) W_T and W_H for T and H along ΔWF, and charge transfer (CT) for all four compounds.

	$NbSe_2$	NbS_2	$TaSe_2$	TaS_2
$\|\vec{u}_A\|$ (Å)	0.00	0.00	0.00	0.00
$\|\vec{u}_B\|$ (Å)	0.26	0.21	0.26	0.20
$\|\vec{u}_C\|$ (Å)	0.32	0.28	0.31	0.25
d (Å)	7.37	6.89	7.51	7.10
W_T (eV)	5.25	5.47	5.02	5.19
W_H (eV)	5.57	6.13	5.45	5.57
ΔWF (eV)	0.32	0.66	0.43	0.77
CT (e)	0.12	0.23	0.14	0.26

The work function results in Table I are consistent with Ref. [34], which reported work function values of $W = 5.35$ eV for T-TaS_2 in the CDW state and $W = 6.07$ eV for H-TaS_2 in the 3×3 CDW state. Here we calculated $W = 5.19$ eV for T-TaS_2 in the CDW state and $W = 5.57$ eV for H-TaS_2 without CDW. We opted not to include the 3×3 CDW state in H-TaS_2 layers in our calculations due to the excessive computational cost of a unit cell commensurate with both $\sqrt{13}\times\sqrt{13}$ and 3×3 CDW states. However, our analysis of the charge transfer as a function of work function differences (ΔWF) suggests this is a good approximation.

D. Charge transfer

Charge transfer (CT) is the central result of this work. To calculate the charge transfer between the different constituents of a heterostructure we followed the method presented in Refs. [34,57]. This method is based on computing the charge density of the full structure with respect to that of a hypothetical reference structure built from the calculated charge densities of the isolated constituents, positioned in the places they would occupy in the full structure. The choice of this method relies on two main pillars: First, it needs only the main output from DFT calculations (i.e., charge density) with small processing, letting our systematic approach be performed without calculation overhead. Second, as shown in Refs. [34,57], it can provide a quantitative measurement for charge transfer. More explicitly, if we consider $\hat{z}$ as the stacking direction, we can obtain the plane-averaged charge density from the self-consistent calculations $\rho_{\text{all}}(z)$ and $\rho_{\text{i}}(z)$, with $i = 1, 2, \ldots, N$, where N is the number of components,

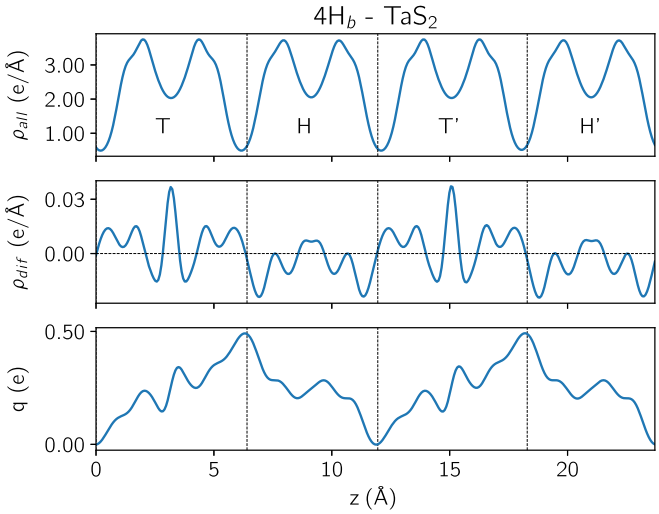

FIG. 3. Electronic density (top), electronic density difference (middle), and total charge change (bottom) for $4H_b$-TaS_2. Zeros for the electronic density difference and thus candidates for z_1/z_2 are marked by vertical dashed lines.

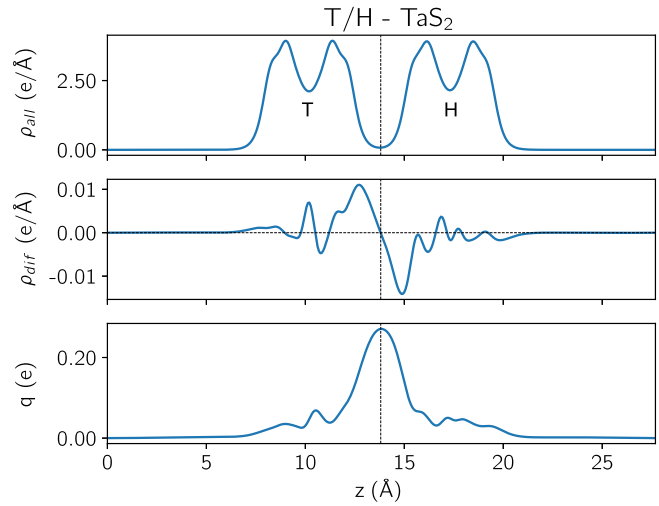

FIG. 4. Electronic density (top), electronic density difference (middle), and total charge change (bottom) for the T/H TaS_2 bilayer. The zero for the electronic density difference is marked by a vertical dashed line.

and obtain the overall charge density difference as

$$\rho_{\text{dif}}(z) = \rho_{\text{all}}(z) - \sum_{i=1}^{N} \rho_i(z). \tag{2}$$

Integrating $\rho_{\text{dif}}(z)$, we can obtain the total charge difference in a section (z_1, z_2) as

$$q_{\text{dif}}(z_1, z_2) = \int_{z_1}^{z_2} \rho_{\text{dif}}(z)\text{d}z. \tag{3}$$

Determining appropriate values for z_1 and z_2 can be challenging when $N > 2$ or for periodic systems, such as the $4H_b$ structure. A practical approach is to set z_1 as the point where $\rho_{\text{dif}}(z_1) = 0$ closest to the interface with the preceding component and z_2 as the point where $\rho_{\text{dif}}(z_2) = 0$ closest to the interface with the subsequent component. For instance, in Fig. 3, the total charge difference for the T layer in $4H_b$ is obtained by integrating from $z_1 = 0$ Å to $z_2 = 6.40$ Å (where the vertical and horizontal dashed lines first intersect in the middle graph); for H, integration ranges from $z_1' = z_2 = 6.40$ Å to $z_2' = 11.95$ Å and so forth. These integration limits correspond to the maximum and minimum values of $q(0, z)$, as illustrated in the bottom graph. In the scenario with $N = 2$ isolated components, integration simplifies: As depicted in Fig. 4, z_1 may be positioned anywhere in vacuum, while $z_2 =$ 2 marks the point where $\rho_{\text{dif}}(z_2) = 0$ closest to the interface. $q(z_1, z_2)$ represents the total charge difference for the first component and the overall absolute charge transfer between components.

In Table I we present the charge transfer results for the relaxed interlayer distances. These distances are 6.89 Å for NbS_2, 7.37 Å for $NbSe_2$, 7.10 Å for TaS_2, and 7.51 Å for $TaSe_2$. Those values are plotted in Fig. 5, where the previously mentioned CT $\propto \Delta$WF trend is clear. From these results, we can detect some trends: *ab initio* calculations predict Ta compounds have greater charge transfer than Nb compounds and S compounds have greater charge transfer than Se compounds.

E. van der Waals effect

In this section, we compare the calculation of the charge transfer with and without van der Waals corrections for the T/H structures obtained in Sec. II D. To do so we incorporate van der Waals corrections into the electronic self-consistent calculations and repeat the charge transfer calculations in Sec. II D. Our findings indicate that these corrections have a negligible influence on charge transfer, typically on the order of $<10^{-3}$.

While van der Waals corrections therefore do not affect charge transfer directly, they could do so indirectly if we performed a new relaxation of the structure in the presence of such corrections since the interlayer distance could change upon relaxation. Since our main interest in this work is to establish relative trends in charge transfer, we instead opted to study charge transfer as a function of interlayer distance

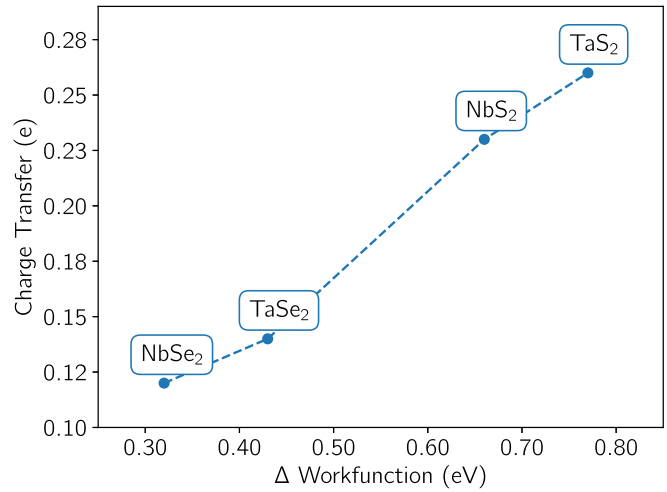

FIG. 5. Charge transfer as a function of the work function difference between layers in the T/H bilayer.

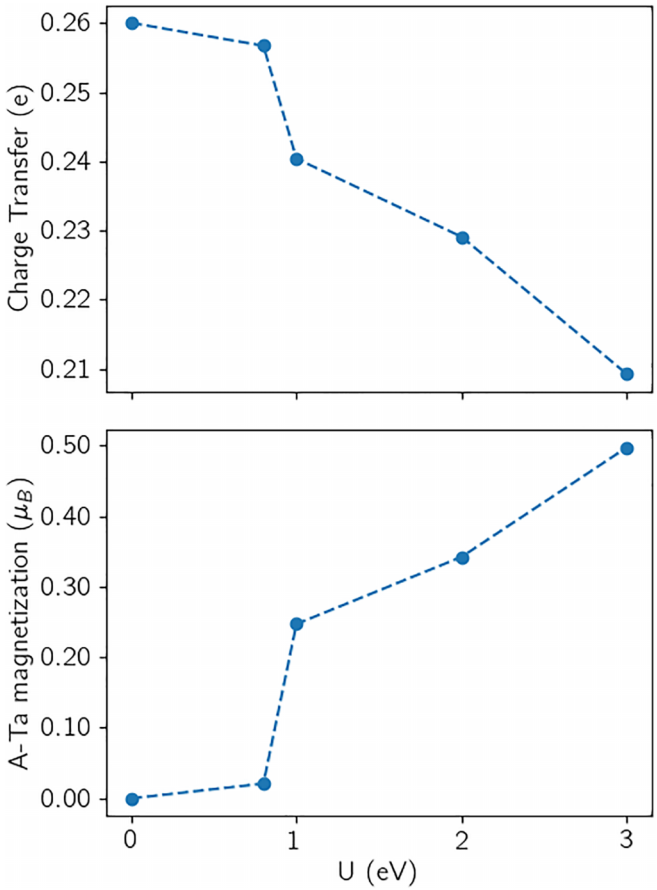

FIG. 6. Charge transfer (top) and magnetization of A atoms in the T layer (bottom) depending on U for TaS_2.

without attempting to calculate precisely its equilibrium value, as this is a more complex problem that depends on both calculational details and experimental conditions.

F. U dependence

Following the same logic as in the previous section, we now consider the effect of the Hubbard interaction U only at the level of electronic self-consistent calculations, keeping the structure fixed [58]. We considered only TaS_2 as an example. The main effect of the Hubbard interaction is to magnetize the flat band near the Fermi level, producing a spin splitting and pushing one of the spin polarizations above the Fermi level. Since a larger magnetization is produced when the lower spin-split band is closer to half filling, increasing U generally leads to a reduction in charge transfer to gain energy from magnetization. The effect should thus be larger in the compound with larger charge transfer, which is TaS_2. Figure 6 illustrates both the charge transfer and magnetization of the center of the SOD as a function of U for this compound. As expected, charge transfer exhibits an inverse relationship with U, although the overall impact of U on charge transfer remains relatively minor (on the order of $10^{-2}e$). The critical U for the flat band magnetization is around $U_c \sim 1$ eV, as we can see from the spin split bands in Appendix B, where we also include a brief comment on the effect of U on the electronic band structures. The conclusion of this section is

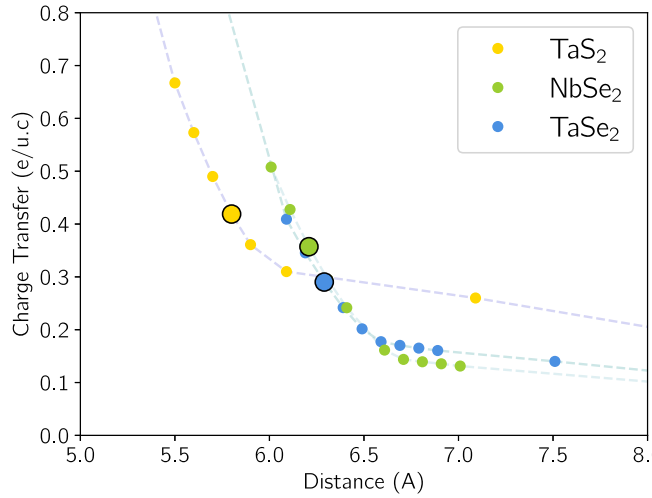

FIG. 7. Charge transfer dependence on interlayer distance for T/H bilayers of $NbSe_2$, TaS_2, and $TaSe_2$ in the nonmagnetic state at $U = 0$. Experimental equilibrium distances for $4H_b$ compounds are marked by a larger dot with a black contour (for $NbSe_2$ an extrapolated value is used; see text).

that while U might have a sizable effect on the bands and magnetization, it is not as relevant for charge transfer.

G. Distance dependence

In order to explore the impact of interlayer distance on charge transfer, we calculated the charge transfer across a range of distances for experimentally reported compounds, encompassing both the relaxed values and those derived from experimental data. The structure of each layer, obtained after relaxation, was kept fixed as the interlayer distance is varied, as we expected the effect of further relaxation to be minimal except, perhaps, at very close distances. Experimental values were determined based on the reported interlayer spacings in bulk $4H_b$ materials. Specifically, for TaS_2 ($c = 23.73$ Å) [22], the Ta-Ta interlayer distance is 5.93 Å. Likewise, for $TaSe_2$ ($c = 25.16$ Å) [59], the corresponding interlayer distance is 6.29 Å. For $NbSe_2$, the $4H_b$ polytype has not been reported, so we extrapolate its interlayer distance by comparison with $TaSe_2$. The interlayer distance in $2H$-$TaSe_2$ is 6.35 Å, which is 1% less than that of $4H_b$-$TaSe_2$ [1]. For $2H$-$NbSe_2$ the interlayer distance is 6.27 Å, so assuming the same trend, we can take 1% less for a hypothetical $4H_b$-$NbSe_2$ structure, i.e., 6.21. NbS_2 was not included in this analysis due to the lack of experimental data. It should be noted that the experimental interlayer distances in bulk compounds need not be the same as for bilayers on a substrate, so these values should be taken only as reference. In general, we also see that these values are smaller than those obtained from relaxation in Table I.

Figure 7 illustrates the interlayer distance dependence of charge transfer for $NbSe_2$, TaS_2, and $TaSe_2$. All three compounds exhibit a comparable trend in charge transfer as a function of distance, characterized by two distinct patterns: At larger interlayer distances, a gradual linear increase in charge transfer is observed, while at smaller distances, a tipping point is reached, beyond which the rate of linear growth becomes more pronounced. From distances of 5.5 Å or less, our charge

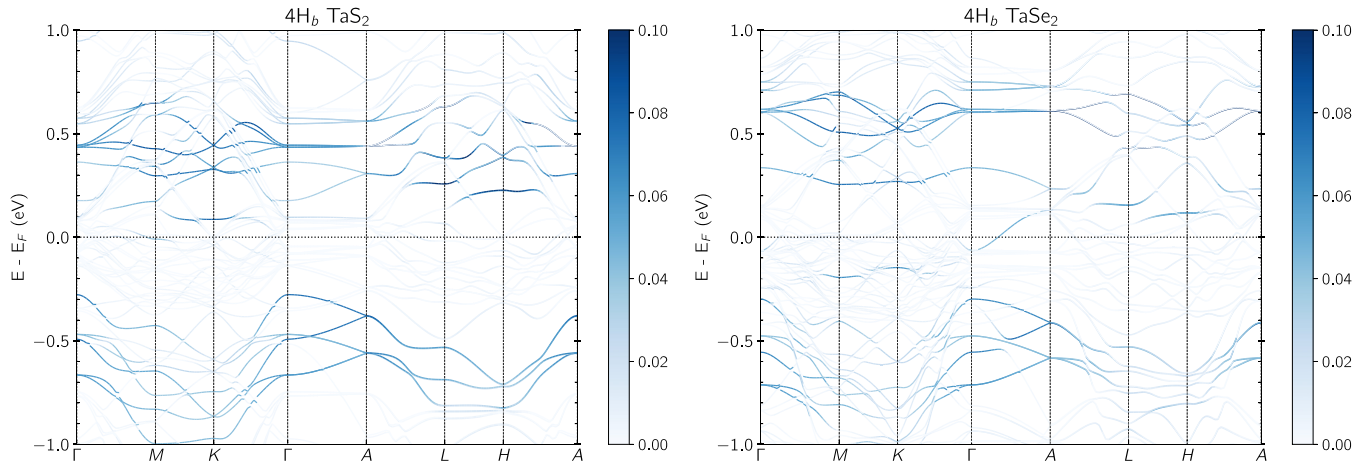

FIG. 8. Band structures for $4H_b$-TaS_2 (left) and $4H_b$-$TaSe_2$ (right) in the structure when the T layer is in the CDW state, color coded by the weight of the wave function in the central SOD atom A. The SOD centers for both T layers are on top of each other.

transfer calculation method becomes less reliable due to the ambiguity in defining the boundaries between subsystems in the presence of strong hybridization. We also observe that TaS_2 has the largest charge transfer also at the experimental interlayer distance.

In order to contextualize our findings within the existing literature, we can now compare them by extrapolating to various distances. For instance, the results reported in Ref. [10] predict a charge transfer of $0.32e$ for $TaSe_2$ at an interlayer distance of 6.60 Å, which exceeds our result of around $0.20e$. Conversely, the investigation of $NbSe_2$ conducted in Ref. [35], where the interlayer distance is 6.08 Å, indicates a charge transfer of $0.17e$, lower than our predicted value of $0.43e$. Reference [30] undertook a similar analysis for TaS_2 but predicted higher overall charge transfers and a smoother evolution towards CT = 1 at small distances, rather than the two-step dependence observed in our results. This disparity may arise from differences in the methods used to calculate charge transfer as well as in the relaxation procedure since Ref. [30] performed a relaxation for each distance, which becomes progressively more important as interlayer hybridization increases. Our work is, however, generally consistent with the fact that interlayer distance is the key parameter that most strongly affects charge transfer, as put forward in Ref. [30].

III. RESULTS: BULK $4H_b$ POLYTYPES

To compare our results with the results obtained from bilayers, we calculated the charge transfer in $4H_b$-TaS_2 and $4H_b$-$TaSe_2$. We constructed the lattice structure in the CDW state by stacking the relaxed structures obtained from single layers in Sec. II A using experimentally reported interlayer distances.

The charge transfer results for $4H_b$ structures of TaS_2 and $TaSe_2$ compounds are $0.49e$/u.c. and $0.39e$/u.c., respectively. These outcomes exhibit consistency with those reported for bilayers and their distance dependence in the preceding sections. To understand these results we also show the band structure projected to the A atom of the SOD in Fig. 8, as well as the partial density of states (DOS) calculations for the A, B, and C atoms in Fig. 9, for the $4H_b$ structures of both compounds. Interestingly, TaS_2 displays a flat band which is above the Fermi level almost everywhere, consistent with a peak in the DOS for the A atom in the range 0–0.4 eV. Taken at face value Fig. 9 would suggest a charge transfer of nearly $1e$/u.c. Similarly, in $TaSe_2$, the flat bands begin at $E \approx 0.3$ eV and $E \approx -0.2$ eV, with the latter seeming to hybridize and reach $E \approx 0.1$ eV after Γ, where it exhibits a higher DOS, as illustrated in Fig. 9. Charge transfer is harder to quantify in this case, but it also appears larger than the computed value of 0.39. These disparities lead us to consider two potential explanations: First, the behavior of bands away from the high-symmetry k path has a significant influence on charge transfer, as there might be bands with significant weight in the A atom below the Fermi level that we simply do not see in the high-symmetry path. Alternatively, interlayer hybridization might already be strong enough that charge transfer cannot be inferred directly from the population of the projected bands, and the computed numerical values should be taken as the reliable ones.

IV. CONCLUSION

In this work, we conducted a detailed *ab initio* study of charge transfer in T/H bilayers of MX_2 and $4H_b$-TaX_2 structures (M=Nb, Ta, X=S, Se), revealing its dependence on Hubbard U, van der Waals corrections, and interlayer distance. The most significant findings are summarized in Table I and illustrated in Fig. 7. Our results indicate that both U and van der Waals corrections have minimal impact on charge transfer, despite finite magnetization. In line with previous work for TaS_2 [30], we found the interlayer distance to be the parameter on which charge transfer is most strongly dependent.

The main result of our work is the revelation of the different trends across T/H compounds. Generally, X = Se compounds exhibit higher charge transfer than those with X = S, while M=Ta compounds also demonstrate greater charge transfer than M = Nb counterparts. Additionally, our method predicts charge transfer is more pronounced in bulk $4H_b$ structures when compared to bilayers. These findings may have important experimental implications. First, there are

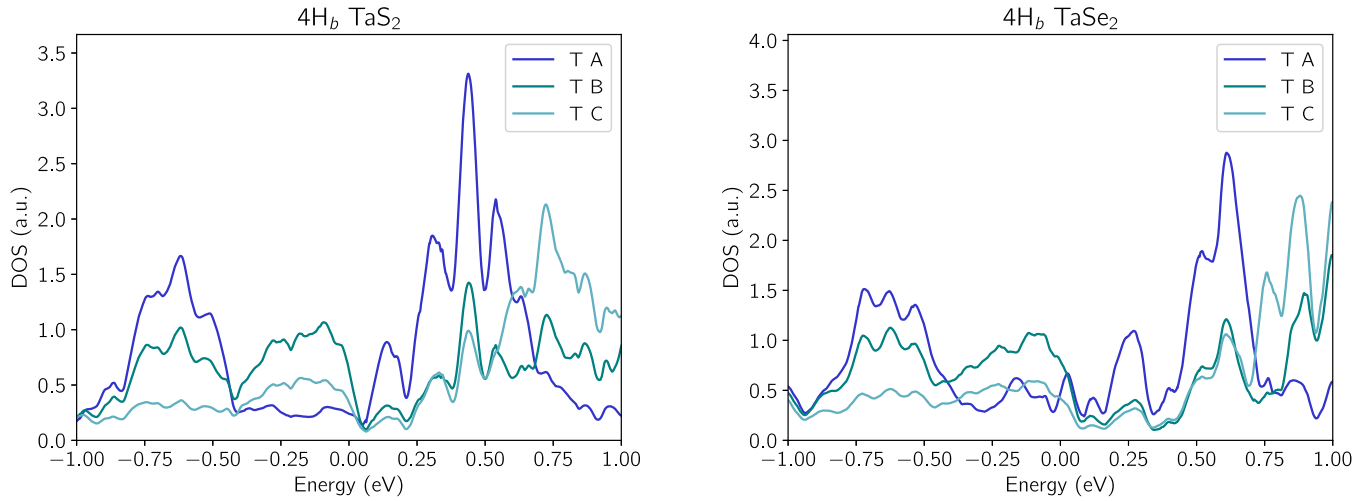

FIG. 9. Atom-projected DOS for the $4H_b$-TaS_2 (left) and $4H_b$-$TaSe_2$ (right) structures for Ta atoms A, B, and C in the Star of David structure in the T layers.

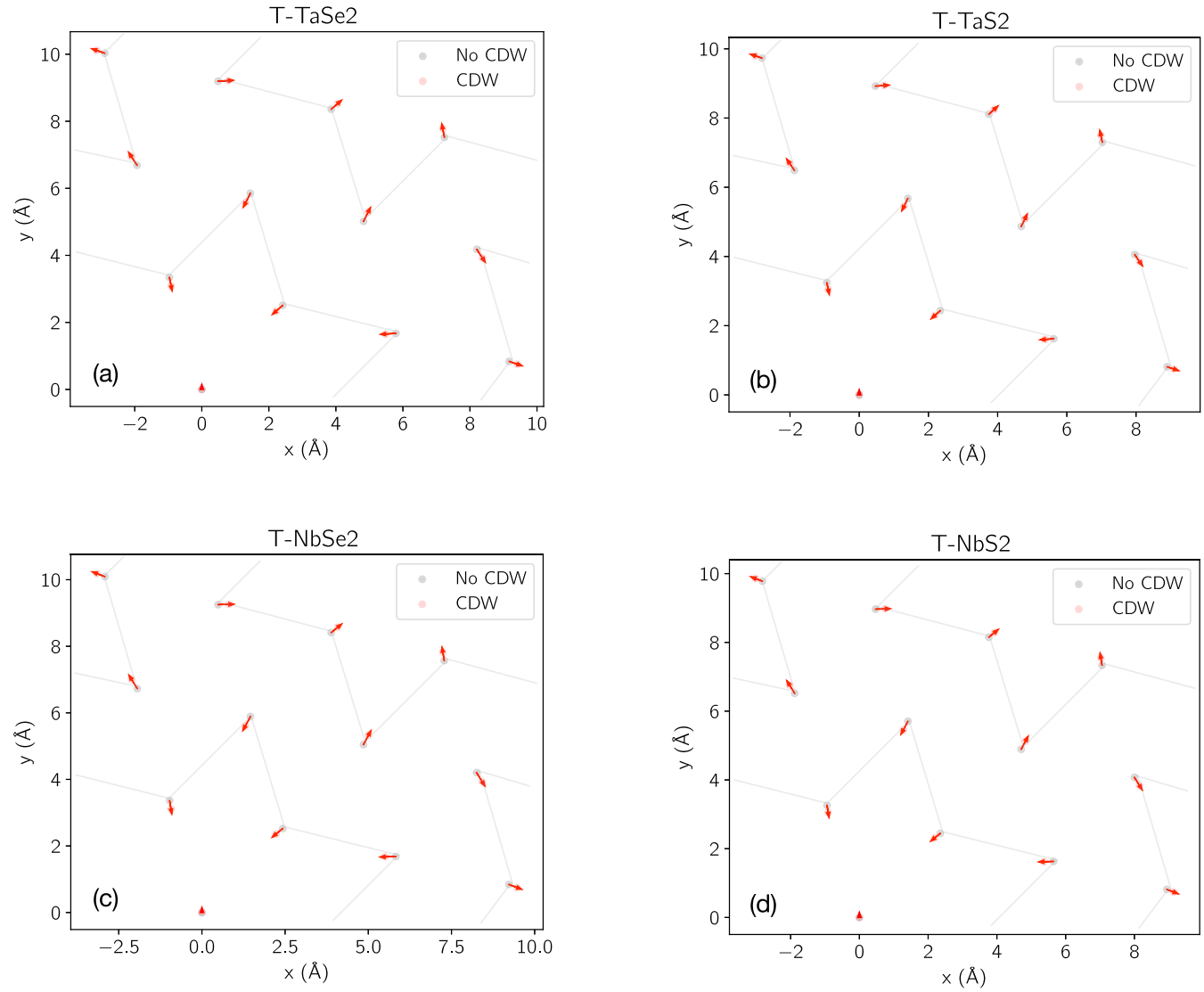

FIG. 10. Atomic positions and displacements of (a) T-$TaSe_2$, (b) T-TaS_2, (c) T-$NbSe_2$, and (d) T-NbS_2 with and without CDW. The SOD CDW its superimposed in order to show the different symmetry positions (A, B, and C).

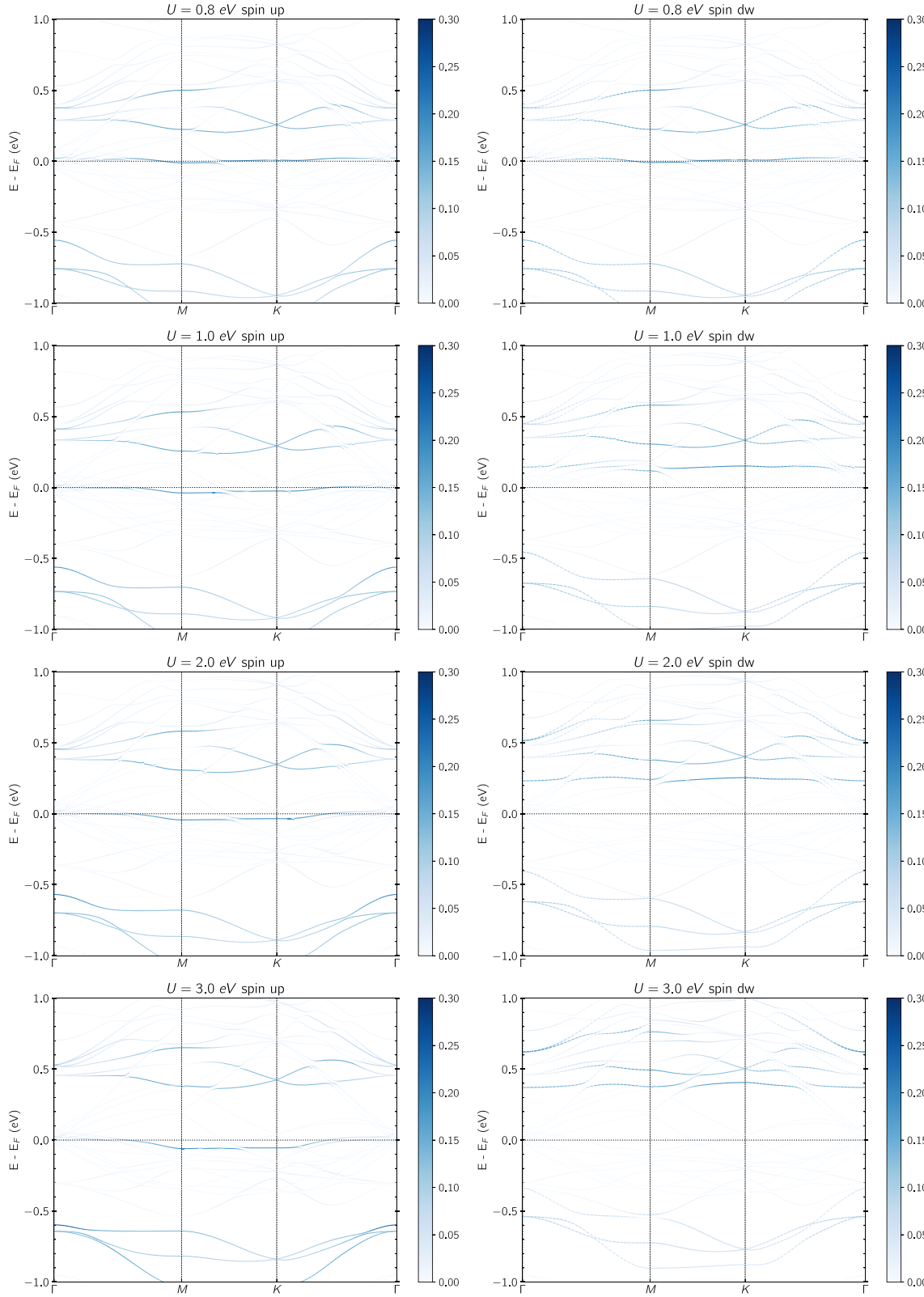

FIG. 11. T/H-TaS_2 electronic atom-projected (onto T's A atom) band structures for the different values of U considered in the main text and both spin polarizations.

clear differences in the behavior of the Kondo peak in T/H bilayers in $TaSe_2$ [9,10], TaS_2 [11,12], and $NbSe_2$ [13,14], as well as in the orbital character of the higher-energy states [9]. Rather than inconsistencies between experiments, these features may reveal that charge transfer and the proximity to the potential Mott insulator state may be different across compounds, and more work is needed to determine charge transfer for each of them experimentally. Similarly, $4H_b$-TaS_2 appears to have larger CT with more clear evidence of a nearly unoccupied flat band [19,20,24], which plays a minor role in superconductivity, but our calculations suggest the flat band might be more populated in $4H_b$-$TaSe_2$ and might have a stronger effect on the superconducting state [60–62]. We hope that our results will stimulate further work to experimentally map out charge transfer across the family of T/H structures, which will lead to a deeper understanding of the unconventional magnetic and superconducting properties in this family of materials.

ACKNOWLEDGMENTS

We acknowledge useful discussions with M. Ugeda and M. Gastiasoro. F.d.J. is supported by Grant No. PID2021-128760NB0-I00 from the Spanish MCIN/AEI/10.13039/501100011033/FEDER, EU. M.G.V. and I.S.-R. acknowledge support from the Deutsche Forschungsgemeinschaft (DFG, German Research Foundation) GA3314/1-1-FOR 5249 (QUAST) and from the Spanish Ministerio de Ciencia e Innovacion Grant No. PID2022-142008NB-I0. M.G.V. acknowledges partial support from the European Research Council (ERC) under Grant Agreement No. 101020833.

APPENDIX A: DISPLACEMENTS

We present the positions for configurations with and without CDW along the displacements for all four TMDs in Fig. 10. All relaxed CDW systems were obtained from a calculation whose initial state had small displacements following the trend of our previous work [10].

APPENDIX B: U BANDS

In this Appendix, we include the spin-projected electronic band structures from the TaS_2 bilayer for all four different U values (see Fig. 11). We can determine that the overall effect of U is to split the T flat band, pushing the spin up band below the Fermi energy and the spin down one up into valence bands, thus increasing magnetization of this band and hindering the charge transfer.

[1] V. L. Kalikhman and Y. S. Umanskĭ, Transition-metal chalcogenides with layer structures and features of the filling of their brillouin zones, Sov. Phys. Usp. **15**, 728 (1973).
[2] J. A. Wilson, F. J. Di Salvo, and S. Mahajan, Charge-density waves and superlattices in the metallic layered transition metal dichalcogenides, Adv. Phys. **24**, 117 (1975).
[3] K. Rossnagel, On the origin of charge-density waves in select layered transition-metal dichalcogenides, J. Phys.: Condens. Matter **23**, 213001 (2011).
[4] As is often done, we label the two-dimensional polytypes with the letters T and H and the bulk polytypes as $1T$, $2H$, $4H_b$, …, where the number refers to the number of layers in the unit cell.
[5] P. Fazekas and E. Tosatti, Charge carrier localization in pure and doped 1T-TaS_2, Phys. B+C (Amsterdam) **99**, 183 (1980).
[6] K. Rossnagel and N. V. Smith, Spin-orbit coupling in the band structure of reconstructed $1T$-TaS_2, Phys. Rev. B **73**, 073106 (2006).
[7] K. T. Law and P. A. Lee, 1T-TaS_2 as a quantum spin liquid, Proc. Natl. Acad. Sci. USA **114**, 6996 (2017).
[8] T. Ritschel, H. Berger, and J. Geck, Stacking-driven gap formation in layered $1T$-TaS_2, Phys. Rev. B **98**, 195134 (2018).
[9] W. Ruan *et al.*, Evidence for quantum spin liquid behaviour in single-layer 1T-$TaSe_2$ from scanning tunnelling microscopy, Nat. Phys. **17**, 1154 (2021).
[10] W. Wan, R. Harsh, A. Meninno, P. Dreher, S. Sajan, H. Guo, I. Errea, F. de Juan, and M. M. Ugeda, Evidence for ground state coherence in a two-dimensional Kondo lattice, Nat. Commun. **14**, 7005 (2023).
[11] V. Vaňo, M. Amini, S. C. Ganguli, G. Chen, J. L. Lado, S. Kezilebieke, and P. Liljeroth, Artificial heavy fermions in a van der Waals heterostructure, Nature (London) **599**, 582 (2021).
[12] C. G. Ayani, M. Pisarra, I. M. Ibarburu, M. Garnica, R. Miranda, F. Calleja, F. Martín, and A. L. Vázquez de Parga, Probing the phase transition to a coherent 2D Kondo lattice, Small **20**, 2303275 (2024).
[13] M. Liu *et al.*, Monolayer 1T-$NbSe_2$ as a 2D-correlated magnetic insulator, Sci. Adv. **7**, eabi6339 (2021).
[14] S. C. Ganguli, J. L. Lado, and P. Liljeroth, Doped Mott phase and charge correlations in monolayer 1T-$NbSe_2$, arXiv:2401.08296
[15] F. J. Di Salvo, B. G. Bagley, J. M. Voorhoeve, and J. V. Waszczak, Preparation and properties of a new polytype of tantalum disulfide (4Hb-TaS_2), J. Phys. Chem. Solids **34**, 1357 (1973).
[16] F. J. Di Salvo, D. E. Moncton, J. A. Wilson, and S. Mahajan, Coexistence of two charge-density waves of different symmetry in $4Hb$-TaS_2, Phys. Rev. B **14**, 1543 (1976).
[17] A. Achari *et al.*, Alternating superconducting and charge density wave monolayers within bulk 6R-TaS_2, Nano Lett. **22**, 6268 (2022).
[18] S. Pal, P. Bahera, S. R. Sahu, H. Srivastava, A. K. Srivastava, N. P. Lalla, R. Sankar, A. Banerjee, and S. B. Roy, Charge density wave and superconductivity in 6R-TaS_2, Phys. B (Amsterdam, Neth.) **669**, 415266 (2023).
[19] S. Shen *et al.*, Coexistence of quasi-two-dimensional superconductivity and tunable Kondo lattice in a van der Waals superconductor, Chin. Phys. Lett. **39**, 077401 (2022).
[20] A. K. Nayak, A. Steinbok, Y. Roet, J. Koo, I. Feldman, A. Almoalem, A. Kanigel, B. Yan, A. Rosch, N. Avraham, and H. Beidenkopf, First order quantum phase transition in the hybrid metal-Mott insulator transition metal dichalcogenide 4Hb-TaS_2, Proc. Natl. Acad. Sci. USA **120**, e2304274120 (2023).

[21] D. Dentelski, E. Day-Roberts, T. Birol, R. M. Fernandes, and J. Ruhman, Robust gapless superconductivity in 4*Hb*-TaS_2, Phys. Rev. B **103**, 224522 (2021).

[22] A. Ribak, R. M. Skiff, M. Mograbi, P. K. Rout, M. H. Fischer, J. Ruhman, K. Chashka, Y. Dagan, and A. Kanigel, Chiral superconductivity in the alternate stacking compound 4Hb-TaS_2, Sci. Adv. **6**, eaax9480 (2020).

[23] E. Persky, A. V. Bjørlig, I. Feldman, A. Almoalem, E. Altman, E. Berg, I. Kimchi, J. Ruhman, A. Kanigel, and B. Kalisky, Magnetic memory and spontaneous vortices in a van der Waals superconductor, Nature (London) **607**, 692 (2022).

[24] A. K. Nayak *et al.*, Evidence of topological boundary modes with topological nodal-point superconductivity, Nat. Phys. **17**, 1413 (2021).

[25] A. Almoalem, I. Feldman, I. Mangel, M. Shlafman, Y. E. Yaish, M. H. Fischer, M. Moshe, J. Ruhman, and A. Kanigel, The observation of -shifts in the Little-Parks effect in 4Hb-TaS_2, Nat. Commun. **15**, 4623 (2024).

[26] I. Silber *et al.*, Two-component nematic superconductivity in 4Hb-TaS_2, Nat. Commun. **15**, 824 (2024).

[27] R. H. Friend, R. F. Frindt, A. J. Grant, A. D. Yoffe, and D. Jerome, Electrical conductivity and charge density wave formation in 4Hb TaS_2 under pressure, J. Phys. C **10**, 1013 (1977).

[28] A. R. Beal, Optical properties of mixed coordination polytypes of TaS_2 in the photon energy range 0.5-6.0 eV, J. Phys. C **11**, 4583 (1978).

[29] N. J. Doran, G. Wexler, and A. M. Woolley, Fermi surfaces, charge-transfer and charge-density-waves in 4Hb-TaS_2, J. Phys. C **11**, 2967 (1978).

[30] L. Crippa, H. Bae, P. Wunderlich, I. I. Mazin, B. Yan, G. Sangiovanni, T. Wehling, and R. Valentí, Heavy fermions vs doped Mott physics in heterogeneous Ta-dichalcogenide bilayers, Nat. Commun. **15**, 1357 (2024).

[31] A. Almoalem *et al.*, Charge transfer and spin-valley locking in 4Hb-TaS_2, npj Quantum Mater. **9**, 36 (2024).

[32] J.-A. Yan, M. A. D. Cruz, B. Cook, and K. Varga, Structural, electronic and vibrational properties of few-layer 2H- and 1T-$TaSe_2$, Sci. Rep. **5**, 16646 (2015).

[33] J. J. Gao, J. G. Si, X. Luo, J. Yan, Z. Z. Jiang, W. Wang, Y. Y. Han, P. Tong, W. H. Song, X. B. Zhu, Q. J. Li, W. J. Lu, and Y. P. Sun, Origin of the large magnetoresistance in the candidate chiral superconductor 4*Hb*-TaS_2, Phys. Rev. B **102**, 075138 (2020).

[34] Z. Wang *et al.*, Surface-limited superconducting phase transition on 1T-TaS_2, ACS Nano **12**, 12619 (2018).

[35] R. Pico, P. Abufager, I. Hamad, R. Robles, and N. Lorente, Understanding the interlayer coupling in 1T/1H-$NbSe_2$ heterobilayers, Phys. Rev. B **110**, 075427 (2020).

[36] P. Darancet, A. J. Millis, and C. A. Marianetti, Three-dimensional metallic and two-dimensional insulating behavior in octahedral tantalum dichalcogenides, Phys. Rev. B **90**, 045134 (2014).

[37] Q. Zhang, L.-Y. Gan, Y. Cheng, and U. Schwingenschlögl, Spin polarization driven by a charge-density wave in monolayer 1*T*-TaS_2, Phys. Rev. B **90**, 081103(R) (2014).

[38] X.-L. Yu, D.-Y. Liu, Y.-M. Quan, J. Wu, H.-Q. Lin, K. Chang, and L.-J. Zou, Electronic correlation effects and orbital density wave in the layered compound 1*T*-TaS_2, Phys. Rev. B **96**, 125138 (2017).

[39] S. Yi, Z. Zhang, and J.-H. Cho, Coupling of charge, lattice, orbital, and spin degrees of freedom in charge density waves in 1*T*-TaS_2, Phys. Rev. B **97**, 041413(R) (2018).

[40] Y. Chen *et al.*, Strong correlations and orbital texture in single-layer 1T-$TaSe_2$, Nat. Phys. **16**, 218 (2020).

[41] T. Jiang, T. Hu, G.-D. Zhao, Y. Li, S. Xu, C. Liu, Y. Cui, and W. Ren, Two-dimensional charge density waves in TaX_2 (X=S, Se, Te) from first principles, Phys. Rev. B **104**, 075147 (2021).

[42] J. W. Park and H. W. Yeom, Atomic structures and electronic correlation of monolayer 1T-$TaSe_2$, arXiv:2008.05702.

[43] E. Kamil, J. Berges, G. Schönhoff, M. Rösner, M. Schüler, G. Sangiovanni, and T. O. Wehling, Electronic structure of single layer 1T-$NbSe_2$: Interplay of lattice distortions, non-local exchange, and Mott–Hubbard correlations, J. Phys.: Condens. Matter **30**, 325601 (2018).

[44] D. Pasquier and O. V. Yazyev, Charge density wave phase, Mottness, and ferromagnetism in monolayer 1*T*-$NbSe_2$, Phys. Rev. B **98**, 045114 (2018).

[45] C. Tresca and M. Calandra, Charge density wave and spin 1/2 insulating state in single layer 1T-NbS_2, 2D Mater. **6**, 035041 (2019).

[46] K. Zhang, C. Si, C.-S. Lian, J. Zhou, and Z. Sun, Mottness collapse in monolayer 1T-$TaSe_2$ with persisting charge density wave order, J. Mater. Chem. C **8**, 9742 (2020).

[47] D. Pasquier and O. V. Yazyev, *Ab initio* theory of magnetism in two-dimensional 1*T*-TaS_2, Phys. Rev. B **105**, L081106 (2022).

[48] J. Zaanen, G. A. Sawatzky, and J. W. Allen, Band gaps and electronic structure of transition-metal compounds, Phys. Rev. Lett. **55**, 418 (1985).

[49] J. Phillips, J. L. Lado, V. Pardo, and A. O. Fumega, Self-doped flat band and spin-triplet superconductivity in monolayer 1T-$TaSe_{2-x}Te_x$, J. Phys.: Condens. Matter **36**, 385804 (2024).

[50] G. Kresse and J. Furthmüller, Efficient iterative schemes for *ab initio* total-energy calculations using a plane-wave basis set, Phys. Rev. B **54**, 11169 (1996).

[51] G. Kresse and J. Furthmüller, Efficiency of *ab-initio* total energy calculations for metals and semiconductors using a plane-wave basis set, Comput. Mater. Sci. **6**, 15 (1996).

[52] J. P. Perdew, K. Burke, and M. Ernzerhof, Generalized gradient approximation made simple, Phys. Rev. Lett. **77**, 3865 (1996).

[53] S. Grimme, J. Antony, S. Ehrlich, and H. Krieg, A consistent and accurate *ab initio* parametrization of density functional dispersion correction (DFT-D) for the 94 elements H-Pu, J. Chem. Phys. **132**, 154104 (2010).

[54] S. L. Dudarev, G. A. Botton, S. Y. Savrasov, C. J. Humphreys, and A. P. Sutton, Electron-energy-loss spectra and the structural stability of nickel oxide: An LSDA+U study, Phys. Rev. B **57**, 1505 (1998).

[55] M.-T. Huebsch, T. Nomoto, M.-T. Suzuki, and R. Arita, Benchmark for *ab initio* prediction of magnetic structures based on cluster-multipole theory, Phys. Rev. X **11**, 011031 (2021).

[56] U. Herath, P. Tavadze, X. He, E. Bousquet, S. Singh, F. Muñoz, and A. H. Romero, Pyprocar: A python library for electronic structure pre/post-processing, Comput. Phys. Commun. **251**, 107080 (2020).

[57] X. Jiang, T. Yilmaz, E. Vescovo, and D. Lu, Manipulating topological properties in Bi_2Se_3/BiSe/ transition metal dichalcogenide heterostructures with interface charge transfer, Phys. Rev. B **109**, 115112 (2024).

[58] To verify our decision to discard U in the structural relaxation, we conducted a test relaxation using the same procedures as described in Sec. II for $U = 2.0$ eV in TaS_2. We found that the effect of including U on the relaxation only changes ionic positions on the order of 10^{-4}–10^{-5} Å. These results are consistent with the findings of Crippa *et al.* [30], which suggests that the overall influence of U in DFT calculations for these compounds is small.

[59] R. Morbt and E. Tronc, Atomic displacements in the charge-density wave induced superstructure of 4Hb-$TaSe_2$, Philos. Mag. B **40**, 305 (1979).

[60] Y. Liu, L. J. Li, W. J. Lu, R. Ang, X. Z. Liu, and Y. P. Sun, Coexistence of superconductivity and commensurate charge density wave in $4H_b$-$Tas_{2-x}Se_x$ single crystals, J. Appl. Phys. **115**, 043915 (2014).

[61] Z. Xie, M. Yang, Z. G. Cheng, T. Ying, J.-G. Guo, and X. Chen, A revisit of superconductivity in $4H_b$-$TaS_{2-2x}Se_{2x}$ single crystals, J. Phys. Soc. Jpn. **92**, 054702 (2023).

[62] Q. Liu, P. Sun, F. Meng, Y. Geng, Z. Liu, J. Zhang, J. Gao, Z. Jiang, S. Tian, X. Luo, Y. Sun, Z. Cheng, K. Liu, H. Lei, and S. Wang, Existence of an ultraflat band in the charge density wave state of $4H_b$-$TaS_{1.3}Se_{0.7}$, Phys. Rev. B **108**, 115115 (2023).